bioRxiv preprint doi: https://doi.org/10.1101/2020.02.26.966762; this version posted February 27, 2020. The copyright holder for this preprint (which was not certified by peer review) is the author/funder, who has granted bioRxiv a license to display the preprint in perpetuity. It is made available under aCC-BY-NC-ND 4.0 International license.

CROSSTALK BETWEEN INVADOPODIA AND THE EXTRACELLULAR MATRIX

Shinji Iizuka[1,4], Ronald P. Leon[1], Kyle P. Gribbin[1], Ying Zhang[2], Jose Navarro[1], Rebecca Smith[2], Kaylyn Devlin[2], Lei G. Wang[2], Summer L. Gibbs[2,3], James Korkola[2,3], Xiaolin Nan[2,3] & Sara A. Courtneidge[1,2,3]

Departments of Cell, Developmental and Cancer Biology[1] and Biomedical Engineering[2], Knight Cancer Institute[3], Oregon Health and Science University, Portland, Oregon, USA

[4]Corresponding author (iizukas@ohsu.edu)

bioRxiv preprint doi: https://doi.org/10.1101/2020.02.26.966762; this version posted February 27, 2020. The copyright holder for this preprint (which was not certified by peer review) is the author/funder, who has granted bioRxiv a license to display the preprint in perpetuity. It is made available under aCC-BY-NC-ND 4.0 International license.

ABSTRACT

The scaffold protein Tks5α is required for invadopodia-mediated cancer invasion both *in vitro* and *in vivo*. We have previously also revealed a role for Tks5 in tumor cell growth using three-dimensional (3D) culture model systems and mouse transplantation experiments. Here we use both 3D and high-density fibrillar collagen (HDFC) culture to demonstrate that native type I collagen, but not a form lacking the telopeptides, stimulated Tks5-dependent growth, which was dependent on the DDR collagen receptors. We used microenvironmental microarray (MEMA) technology to determine that laminin, collagen I, fibronectin and tropoelastin also stimulated invadopodia formation. A Tks5α-specific monoclonal antibody revealed its expression both on microtubules and at invadopodia. High- and super-resolution microscopy of cells in and on collagen was then used to place Tks5α at the base of invadopodia, separated from much of the actin and cortactin, but coincident with both matrix metalloprotease and cathepsin proteolytic activity. Inhibition of the Src family kinases, cathepsins or metalloproteases all reduced invadopodia length but each had distinct effects on Tks5α localization. These studies highlight the crosstalk between invadopodia and extracellular matrix components, and reveal the invadopodium to be a spatially complex structure.

Keywords: Tks adaptors, proteases, invadopodia, actin, extracellular matrix, super-resolution microscopy

bioRxiv preprint doi: https://doi.org/10.1101/2020.02.26.966762; this version posted February 27, 2020. The copyright holder for this preprint (which was not certified by peer review) is the author/funder, who has granted bioRxiv a license to display the preprint in perpetuity. It is made available under aCC-BY-NC-ND 4.0 International license.

INTRODUCTION

Cancer invasion, the ability of cancer cells to infiltrate into and through extracellular matrix (ECM), has long been associated with tumor metastasis (Hanahan and Weinberg, 2011). Increasing evidence suggests that the same mechanisms that allow invasive capacity also promote tumor growth during cancer progression. This may be because the ECM acts as a physical barrier to tumor growth, which cancer cells destroy by activating pericellular proteases (Lu et al., 2012), Alternatively, these same pericellular proteases can release latent growth factors and cytokines in the matrix that promote tumor growth and angiogenesis (Chang and Werb, 2001). In either case, tumor growth and tumor metastasis are interlinked.

In many types of cancer, degradation of ECM has been linked to the formation of invadopodia (Murphy and Courtneidge, 2011; Weaver, 2008b), actin-rich plasma membrane protrusions coordinate the cytoskeleton with pericellular proteolytic activity. Since their discovery, invadopodia have been considered characteristic structures of invasive disease. Aside from an array of actin-regulatory proteins and signaling molecules, invadopodia also contain several classes of protease, including members of the metalloprotease superfamily (Chang and Werb, 2001; Seals and Courtneidge, 2003), serine proteases such as fibroblast activation protein (FAP) (Monsky et al., 1994) and urokinase-type plasminogen activator (uPA) and its receptor (uPAR) (Artym et al., 2002), and cysteine proteases such as cathepsins (Tu et al., 2008). Despite our steadily increasing knowledge of the composition and functions of invadopodia *in vitro*, much less is known about their *in vivo* presence and functional relevance *in vivo*. However, related podosome structures have been observed in motile vascular smooth muscle cells and neural crest stem cells *in vivo* (Murphy et al., 2011; Quintavalle et al., 2010), and genetically-defined invadopodia have been observed during intra- and extra-vasation in animal models (Gligorijevic et al., 2014; Leong et al., 2014) as well as in freshly explanted primary human tumors (Weaver, 2008a).

bioRxiv preprint doi: https://doi.org/10.1101/2020.02.26.966762; this version posted February 27, 2020. The copyright holder for this preprint (which was not certified by peer review) is the author/funder, who has granted bioRxiv a license to display the preprint in perpetuity. It is made available under aCC-BY-NC-ND 4.0 International license.

Almost all of the components of invadopodia are also found in other actin-based structures such as adhesion complexes and protrusions (Murphy and Courtneidge, 2011). However, the Tks5 adaptor protein (SH3PXD2A) has a more restricted subcellular distribution, and is found predominantly at invadopodia (Saini and Courtneidge, 2018). Furthermore, knockdown of Tks5 prevents invadopodia formation and function (Abram et al., 2003; Buschman et al., 2009; Iizuka et al., 2016; Seals et al., 2005). Conversely, enforced expression of the longest, α isoform of Tks5 in non-invasive cancer cells lacking native expression results in the formation of invadopodia (Seals et al., 2005). Together these data support the conclusion that Tks5α is an obligate invadopodia scaffold, and its expression can be used as a surrogate to study invadopodia-based invasive capacity.

The Tks5 and related Tks4 adaptors are large scaffolding proteins composed of phosphatidylinositol lipid binding PX domains followed by 5 or 4 SH3 domains respectively. Both adaptors are Src substrates, and also contain multiple serine/threonine phosphorylation motifs. While we do not yet have a full understanding of all binding partners of the Tks adaptors, they have been implicated in reactive oxygen species (ROS) production (Diaz et al., 2009) and have been shown to interact with actin-remodeling proteins (Crimaldi et al., 2009; Oikawa et al., 2008; Stylli et al., 2009), pericellular proteases (Buschman et al., 2009), as well as the small GTPase Rab40b (Jacob et al., 2016), the guanine exchange factor Sos1, and the membrane remodeling GTPase dynamin (Rufer et al., 2009). The Oikawa lab has shown that invadopodium formation is initiated near focal adhesions by the binding of the Tks5α PX domain to $PI3,4P_2$ (Oikawa et al., 2008). This model was refined by Condeelis *et al.*, who showed that small actin foci form in the absence of Tks5 (likely following Src phosphorylation of cortactin), and that Tks5 acts to stabilize these nascent protrusions (Sharma et al., 2013). However, few studies to date have examined

bioRxiv preprint doi: https://doi.org/10.1101/2020.02.26.966762; this version posted February 27, 2020. The copyright holder for this preprint (which was not certified by peer review) is the author/funder, who has granted bioRxiv a license to display the preprint in perpetuity. It is made available under aCC-BY-NC-ND 4.0 International license.

70 the structure and function of invadopodia formed *in vitro* in response to extracellular matrix, where

71 their full functionality is observed. Here we describe such experiments.

72

73

bioRxiv preprint doi: https://doi.org/10.1101/2020.02.26.966762; this version posted February 27, 2020. The copyright holder for this preprint (which was not certified by peer review) is the author/funder, who has granted bioRxiv a license to display the preprint in perpetuity. It is made available under aCC-BY-NC-ND 4.0 International license.

MATERIALS AND METHODS

Cell lines

The luciferase-expressing human breast cancer cell line MDA-MB-231-Luc was obtained from Xenogen. The Src-transformed NIH-3T3 (Src3T3) cells have been described previously (Seals et al., 2005). The cell lines were routinely cultured in Dulbecco's minimal essential medium (DMEM) supplemented with 10% Fetal Bovine Serum (FBS) and a cocktail of penicillin and streptomycin (P/S) (Gibco). The human breast cancer cell lines, Hs578t and HCC1806, UACC812, SUM44PE, SUM52PE, HCC1187, SUM1315MO2, HCC1143, HCC1937, BT474 and HCC3153 were kindly provided by Dr. Joe Gray (Oregon Health and Science University [OHSU], USA). The culture medium used: SUM52PE (HAMS F12, 5% FBS, 1M HEPES, 1mg/mL hydrocortisone, 10mg/mL Insulin), HCC1187 (RPMI, 10% FBS), SUM1315MO2 (HAMS F12, 10ug/mL EGF, 5% FBS, 10mM HEPES, 5ug/mL insulin), HCC1143 (RPMI, 10% FBS), HCC1937 (RPMI, 10% FBS), BT474 (DMEM, 10%FBS) and HCC3153 (DMEM, 10%FBS).

DNA constructs and shRNAs

Human Tks5α was cloned into pCDH-CMV-MCS-EF1-Puro (Addgene) with a GFP sequence fused at the C-terminus. The shRNAs pLKO.1 lentiviral plasmids used for scrambled and human Tks5 knockdown were described previously (Blouw et al., 2015). The clones used were TRCN136336 (D5), TRCN0000136014 (D6) and TRCN0000136512 (D7). The shRNAs pLKO.1 lentiviral plasmids used for DDR1 and DDR2 knockdown were: TRC000121082 and TRCN0000361395. The plasmids encoding cortactin (#26722), N-WASP (#54199) and fascin (#54094) were obtained from Addgene. Each insert was cloned into the lentiviral plasmid pCDH-CMV-MCS-EF1-Puro with GFP fusion protein at C-terminus.

Tks5 antibodies design and production

bioRxiv preprint doi: https://doi.org/10.1101/2020.02.26.966762; this version posted February 27, 2020. The copyright holder for this preprint (which was not certified by peer review) is the author/funder, who has granted bioRxiv a license to display the preprint in perpetuity. It is made available under aCC-BY-NC-ND 4.0 International license.

The antibodies for Tks5 (Rabbit monoclonal, F4 and mouse monoclonal, G6) were generated by Abcam/Epitomics (F4) or by the Oregon Stem Cell Center, Monoclonal Antibody Core Facility at OHSU (G6), and validated by the Courtneidge laboratory. The following primer sets were used for cloning into pGEX-4T1 to produce the immunogens:

PX domain (F4)-Forward: CGGGATCCATGCTCGCCTACTGCGTGCAG

PX domain (F4)-Reverse: CCGCTCGAGCTACTCTTTTGGAGGGTTGACATC

SH-linker (G6)-Forward: CTTCAGAGGATGTGGCCCTG

SH-linker (G6)-Reverse: CCTCACTCTTGGAGCCCTTG

For Protein production: Appropriate DNA constructs were transformed into BL121 E.coli and a single colony was selected and grown overnight at 37 °C in 5 mL of LB medium with ampicillin. The overnight culture was then added to 1 L of LB-ampicillin pre-warmed to 25 °C, grown in a shaking incubator at 25 °C until OD600 was reached 0.5. Follow this, IPTG was added to a final concentration of 0.1mM and cultured overnight at 25 °C. The cells were pelleted in a centrifuge and lysed with lysis buffer (20mM Tris pH 7.5, 1% Triton, 1mg/mL Lysozyme, 5mM DTT and protease inhibitor cocktail, Roche #11-836-170 001) for 1 hour at 4 °C. Lysed cells were placed in pre-cooled tubes in an ice bath, and sonicated at 50% power with Sonic Dismembrator (Model 705, Fisher Scientific) with a micro-tip for 30 seconds, in 5 cycles. Lysates were centrifuged at 10,000xg for 5 minutes at 4 °C and the pellet was discarded. 5 mL of glutathione sepharose 4B was prepared according to manufacturer's instructions (GE #17-0756-01) and added to the lysates, which were incubated at 4 °C on a rocking platform for 3 hours. The lysates were centrifuged at 500xg for 5 min at 4 °C and was washed in 50 mL of ice-cold 1X PBS for a total of three washes then re-suspended in a final volume of 20 mL of ice-cold PBS. An appropriate size of chromatography column (R&D) was loaded with chilled sepharose beads at 4°C and allowed to settle. Lysate solution was added to the column and allowed to pass through the column by

bioRxiv preprint doi: https://doi.org/10.1101/2020.02.26.966762; this version posted February 27, 2020. The copyright holder for this preprint (which was not certified by peer review) is the author/funder, who has granted bioRxiv a license to display the preprint in perpetuity. It is made available under aCC-BY-NC-ND 4.0 International license.

gravity. 5 mL of elution buffer (50mM Tris HCL, 25mM glutathione, pH 8.0) was added to the beads, and this process was repeated for a total of 12-18 cycles. Eluates were collected at each cycle and kept on ice. To determine which elution contained the protein, samples of each elution were loaded onto a poly-acrylamide gel which was stained by coomassie-blue followed by de-stain (Thermo Fisher Scientific). Eluates that contained the appropriate proteins were pooled together in a pre-chilled tube on ice. Pooled eluates were concentrated in an Amicon Ultra (Millipore) centrifuge unit. Purified lysates were immediately frozen at -80 °C to maintain integrity of proteins. GST tagged proteins were verified by immunoblot with an anti-GST antibody (#71-7500, Zymed). Purified lysates were then sent to Abcam/Epitomics (F4), or to the Oregon Stem Cell Center, Monoclonal Antibody Core Facility at OHSU (G6) for production of monoclonal antibodies.

Immunizations for monoclonal antibody production at OHSU was conducted under a protocol approved by the OHSU Institutional Animal Care and Use Committee. Balb/C mice received multiple IP immunizations with the Tks5 protein. Four days after the final boost, mice were humanly euthanized using CO2 and their spleens were harvested. Splenocytes were fused with SP2/0 Ag14 myeloma cells (Kohler and Milstein, 1975) and hybrid cells were selected by growth in methylcellulose-containing HAT medium (Stem Cell Technologies). Approximately 600 clones were isolated and transferred to liquid HT medium in 96-well plates. Supernatants from these wells were initially screened for Tks5-specific monoclonal antibodies by ELISA.

Antibodies and reagents for immunoblotting and staining

Antibodies used for immunoblotting were: F4 (1:10), G6 (1:500) and tubulin (T6557, Sigma, 1:3000). Antibodies used for immunofluorescence staining were: F4 (1:10), G6 (1:250) and tubulin

bioRxiv preprint doi: https://doi.org/10.1101/2020.02.26.966762; this version posted February 27, 2020. The copyright holder for this preprint (which was not certified by peer review) is the author/funder, who has granted bioRxiv a license to display the preprint in perpetuity. It is made available under aCC-BY-NC-ND 4.0 International license.

(6074, 1:250, Sigma). Fluorescently labeled phalloidin (Alexa Fluor-350, -488, -568 or -647, Thermo Fisher Scientific) was used for actin staining. Hoechst (1:4000, Thermo Fisher Scientific) was used for nuclear staining.

Invadopodia assay on high-dense fibrillar type I collagen (HDFC)

Invadopodia staining was performed as previously described (Iizuka et al., 2016). Briefly, cells were grown on glass coverslips with or without collagen and fixed with 4% paraformaldehyde/PBS (Electron Microscopy Sciences). For the invadopodia assay on collagen-coated coverslips, HDFC was prepared according to the original protocol reported (Artym, 2016; Artym et al., 2015). Briefly, 18 mm coverslips were pre-chilled on ice and coated with 10 µl ice-cold neutralized collagen (#35429, Corning). The pipette tip was used to spread the collagen evenly on the glass surface and the coated coverslips were left on ice for 10 min to facilitate flattening of the collagen. The layer of collagen was polymerized into a fibrillar meshwork at 37 °C for 30 min, followed by centrifugation at 3,500 g for 20 min. After fixation and permeabilization with 0.1% Triton X-100/PBS for 15 min, the cells were blocked by 5% BSA in PBS with 5% goat-serum for 1 hour at room temperature (RT) and incubated with primary antibodies for 90 min at RT (or overnight at 4 °C). The cells were washed and incubated with Alexa Fluor-conjugated secondary antibodies and phalloidin. Confocal images were collected using a laser-scanning confocal microscope LSM880 equipped with AiryScan (Carl Zeiss). Images were transferred to Imaris™ (Bitplane) which is a multidimensional analysis program based on the fluorescence intensity data to create 3D view of invadopodia and quantify invadopodia length, which was measured by Imaris software using the polygon scaling tool in Slice view.

2D/3D proliferation assays

bioRxiv preprint doi: https://doi.org/10.1101/2020.02.26.966762; this version posted February 27, 2020. The copyright holder for this preprint (which was not certified by peer review) is the author/funder, who has granted bioRxiv a license to display the preprint in perpetuity. It is made available under aCC-BY-NC-ND 4.0 International license.

Type I collagen 3D cultures were performed as described previously (Iizuka et al., 2016). For collagen 3D proliferation assay, briefly rat-tail type I collagen (#08-115, Sigma, Millipore) was prepared to a final concentration of 2.1 mg/ml, and 2,500 cells were added to the collagen mix before gelling. For atelocollagen proliferation assay, rat-tail type I collagen or atelocollagen (##602, Yo Proteins) was prepared to a final concentration of 2.1 mg/ml and added to multi-well plate for 1hr in a CO_2 incubator. Spread cells were grown in DMEM containing 10% FBS. The matrix was dissolved with 2 mg/ml collagenase type2 (#LS004176, Worthington Biochemical corporation) and cell numbers were quantified using hemocytometry. HDFC was prepared according to original protocol reported in (Artym, 2016; Artym et al., 2015) and described briefly above. The HDFC was dissolved with a 1:1 mixture of 2 mg/ml collagenase type2 and trypsin (Gibco), and cell numbers were quantified using hemocytometry. For the growth assay in Matrigel (BD Biosciences), briefly, the cells were added to Matrigel (1:1 dilution with serum-free medium) on ice before gelling in a CO_2 incubator for 30 min. The cells in Matrigel were cultured in DMEM containing 10% FBS. The matrix was dissolved with cold PBS and cell numbers were quantified by hemocytometry.

Invasion and growth assay and invadopodia staining in spheroids

3D spheroid cultures were performed as described previously (Kelm et al., 2003). Briefly, spheroids of MDA-MB-231 cells were prepared in hanging droplets with 2,000 cells in 10 µl of 20% FBS containing DMEM for 3 days. The spheroids were embedded in 2.1 mg/ml of rat type I collagen (#354263, Corning) and incubated with DMEM containing 10%FBS for 2 days. Spheroids were fixed with 4% PFA and washed with PBS for three times. After permeabilization with 0.1% Triton X-100/PBS for 15 min, the samples were stained by Alexa Fluor-568-phalloidin to visualized the entire spheroid in 3D collagen. Imaging was performed on Zeiss/Yokogawa CSU-X1 spinning disk confocal microscope and the *z*-section with the maximum size of actin stained spheroids

bioRxiv preprint doi: https://doi.org/10.1101/2020.02.26.966762; this version posted February 27, 2020. The copyright holder for this preprint (which was not certified by peer review) is the author/funder, who has granted bioRxiv a license to display the preprint in perpetuity. It is made available under aCC-BY-NC-ND 4.0 International license.

were collected and measured for the "spheroid size (actin intensity)". For invadopodia visualization, spheroids were stained by Alexa Fluor-568-phalloidin and Hoechst (1:4000, Thermo Fisher Scientific, used for nuclear staining). Imaging was performed on a laser-scanning confocal microscope LSM880 equipped with AiryScan. Inhibitors used for the spheroid growth assay were: GM6001 (EMD Millipore), CA074 (Vergent Biosciences) and DDR1-1N-1 (Selleck Chemicals).

Microenvironmental Microarray (MEMA)

MEMAs were produced as described previously (Smith et al., 2019; Watson et al., 2018) with several minor modifications. The same set of 45 ECM or ECM combinations that we previously reported were plated into the bottom of 96 well plates (Ibidi). The plates were left desiccated for several days at room temperature, then 3000 MDA-MB-231 cells containing Tks5αGFP were plated in 100 µl DMEM containing 10% FBS. After overnight adhesion in a 37 °C incubator with 5% CO_2, an additional 100 µl of DMEM containing PBS control, epidermal growth factor (EGF), fibroblast growth factor 2 (FGF2), or hepatocyte growth factor (HGF) was added to give final concentrations of 10 ng/ml EGF and FGF2 and 40 ng/ml of HGF. The cells were left to grow for 24h, then fixed with 4% PFA and washed with PBS three times. The cells on MEMA were stained with Alexa Fluor-568-phalloidin to visualize the invadopodia, which were also marked with Tks5αGFP, where double positive delineated invadopodia). Hoechst was used for staining of cell nuclei. Imaging was performed on laser-scanning confocal microscope LSM880 equipped with AiryScan.

Super resolution microscopy

MDA-MB-231 cells with Tks5αGFP were cultured on HDFC prepared on #1.5 coverglass for 2 days before stained for F-actin (phalloidin-Alexa Fluor-647) and Tks5αGFP (GFP-nanobody,

bioRxiv preprint doi: https://doi.org/10.1101/2020.02.26.966762; this version posted February 27, 2020. The copyright holder for this preprint (which was not certified by peer review) is the author/funder, who has granted bioRxiv a license to display the preprint in perpetuity. It is made available under aCC-BY-NC-ND 4.0 International license.

ChromoTek GFP Vhh, # gt-250) using manufacturer recommended procedures. The GFP-nanobody was conjugated to an oligonucleotide ('P1' docking strand) using published procedures (Schnitzbauer et al., 2017). After staining, the cells were imaged sequentially, first with DNA-PAINT (using a CF660R conjugated 'P1' imager strand) in buffer C, which contains 1x PBS supplemented with 500 mM NaCl. Each time after a cell was imaged with DNA-PAINT, the buffer was replaced with 1x PBS supplemented with an oxygen scavenging mixture (comprising glucose oxidase, catalase, and glucose) and 50 mM 2-mercaptoethylamine (MEA) for STORM imaging (van de Linde et al., 2011). For both DNA-PAINT and STORM imaging, a weak cylindrical lens (f=1000 mm) was inserted in front of the detector (Andor iXon Ultra 897) for 3D single-molecule localization (Huang et al., 2008). DNA-PAINT and STORM imaging were performed on a custom setup as described previously (Creech et al., 2017), and 3D localizations were done using ThunderSTORM (Ovesny et al., 2014).

Activity-base probes (MMP-ABP, CTS-ABP)

Cathepsin activity-base probe (CTS-ABP) were purchased from Vergent Bioscience and imaging was performed according to manufacturer's instructions.

Chemical synthesis of MMP activity-based probe (MMP-ABP): SiTMR (Lukinavicius et al., 2013), 3-azido-1-propanamine (Hannant et al., 2010), and HxBP (Saghatelian et al., 2004) were synthesized following published protocols. To a solution of SiTMR (200 mg, 423 μmol) in DCM (10 mL) at room temperature, DiPEA (442 μL, 2.54 mmol, 6 eq) was added. The reaction was stirred for 10 mins before HOBt (71 mg, 508 μmol, 1.2 eq), 3-azido-1-propanamine (85 mg, 846 μmol, 2 eq) and EDC (97 mg, 508 μmol, 1.2 eq) were added sequentially. The reaction mixture was covered from light and stirred overnight. The reaction was subsequently added saturated $NaHCO_3$ and extracted with DCM (3 × 50 mL). The combined organic layers were rinsed with brine, dried over anhydrous Na_2SO_4, and the solvent was removed using a rotary evaporator. The

bioRxiv preprint doi: https://doi.org/10.1101/2020.02.26.966762; this version posted February 27, 2020. The copyright holder for this preprint (which was not certified by peer review) is the author/funder, who has granted bioRxiv a license to display the preprint in perpetuity. It is made available under aCC-BY-NC-ND 4.0 International license.

245 residue was purified by flash column chromatography with silica gel, using DCM/MeOH as eluent
246 to give compound SiTMR-N_3 (173 mg, 74%) as a pale green solid. Under N_2, compound HxBP
247 (4.2 mg, 7.84 μmol) and SiTMR-N_3 (5 mg, 9.02 μmol) were suspended in 2 ml degassed
248 DMSO/H_2O (1/1, v/v). Freshly prepared 100 mM sodium ascorbate solution (95 μL) and copper
249 sulfate ($CuSO_4$) solution (40 μL) were added to the solution. The resulting reaction mixture was
250 stirred at room temperature overnight and purified using preparative high-performance liquid
251 chromatography (HPLC, Agilent 1250 Infinity HPLC) with a C18 column (150 × 21.2 mm). The
252 sample was eluted using solvents A: water-formic acid (99.9:0.1, v/v) and B: acetonitrile-formic
253 acid (99.9:0.1, v/v), with the gradient increased from 10% B to 90% B over 60 mins at a flowrate
254 of 10 mL/min. The fractions containing product were frozen and lyophilized to afford MMP-ABP
255 (4.1 mg, 48%) as a blue solid. HRMS (ESI-TOF) m/z $[M + 2H]^{2+}$ calculated for $C_{60}H_{71}N_9O_9Si_2$
256 545.7645, found 545.7658. Synthetic route, structure and purity confirmation of MMP-ABP is
257 shown in **Supplementary Figure S1**.

bioRxiv preprint doi: https://doi.org/10.1101/2020.02.26.966762; this version posted February 27, 2020. The copyright holder for this preprint (which was not certified by peer review) is the author/funder, who has granted bioRxiv a license to display the preprint in perpetuity. It is made available under aCC-BY-NC-ND 4.0 International license.

RESULTS AND DISCUSSION

New reagents to study Tks5 isoforms

There are multiple isoforms of Tks5, generated by alternative promoter usage (Cejudo-Martin et al., 2014; Li et al., 2013). The full length (α) isoform contains the amino terminal PX domain (**Figure 1A**) required for phosphatidylinositol lipid binding and the formation of invadopodia (Seals et al., 2005), while the shorter isoforms (β and short) lack this domain. The Tks5-specific antibodies we generated previously (Lock et al., 1998) were raised against the first and third SH3 domains of the mouse protein. As a result, this antibody could not distinguish between the α and β isoforms nor reliably between Tks4 and Tks5; they also did provide high fidelity staining in human cells. To overcome these limitations, we generated new Tks5 antibodies to assist in the study of invadopodia. Of these, F4 is a rabbit monoclonal antibody (produced in collaboration with Epitomics, Inc.) raised against an epitope in the PX domain of Tks5α, and G6 is a mouse monoclonal antibody (produced in collaboration with the Flow Cytometry Shared Resource at OHSU) raised against an epitope in one of the unique linker domains of Tks5. The specificity of these antibodies in immunoblotting is demonstrated in **Figure 1B**. G6 recognizes both full-length and PX domain-deleted forms of Tks5 (e.g., the α and β isoforms) in human cells, whereas F4 recognizes only the full-length α isoform of Tks5. Neither antibody recognized the related Tks4 protein.

Given our interest in the role of invadopodia in breast cancer, we next used the G6 (“panTks5”) antibody to profile a series of invasive human breast cancer cell lines. All tested cell lines expressed predominantly Tks5α, with low levels of Tks5β and short also detected in some cell lines (**Figure 1C**). We examined expression by immunofluorescence in one of these cell lines, MDA-MB-231. Focusing on the ventral surface of the cell, we noted co-localization of G6 with the puncta of F-actin characteristic of invadopodia, as expected, whereas no staining was seen if Tks5 expression was reduced by RNA interference (**Figure 1D**). The F4 antibody also showed

bioRxiv preprint doi: https://doi.org/10.1101/2020.02.26.966762; this version posted February 27, 2020. The copyright holder for this preprint (which was not certified by peer review) is the author/funder, who has granted bioRxiv a license to display the preprint in perpetuity. It is made available under aCC-BY-NC-ND 4.0 International license.

specific staining at invadopodia in these cells (**Figure 1E**). Thus, we conclude that these antibodies are suitable for both immunoblotting and immunocytochemistry. We also found them to provide suitable utility for immunoprecipitation and immunohistochemistry (data not shown). We next used F4 for high-resolution imaging of Tks5α in Src-transformed mouse fibroblasts (Src-3T3), a workhorse for studies on invasive behavior in which the invadopodia form into characteristic rosettes (Chen, 1989; Tarone et al., 1985). Here too we observed Tks5α co-localization with F-actin in the rosettes (**Figure 1F**). However, in these cells, the relative lack of actin stress fibers, coupled with our use of high-resolution microscopy, also allowed us to observe punctate staining of Tks5α in the cytoplasm. Interestingly, in the cytoplasm Tks5α staining was coincident with tubulin, but not actin, suggesting that Tks5α is localized to microtubules as well as invadopodia. Similar distribution was observed when Tks5α fused with GFP or mCherry was expressed in the cells. This analysis also revealed that the microtubules terminated near the rosettes, in keeping with other reports on podosomes and invadopodia (Linder et al., 2011; Luxenburg et al., 2007; Schoumacher et al., 2010). These data suggested the trafficking of Tks5α on microtubules, which indeed we have now observed (studies to be reported elsewhere).

Morphology and growth of breast cancer cells with and without Tks5.

The ECM, particularly collagen-I, can control cell survival, proliferation, migration and invasion. In cancer, collagen-I had been thought to be growth suppressive (Henriet et al., 2000), but this view is now more nuanced (Keely, 2011; Pickup et al., 2014). For example, increased collagen-I density and changed ECM architecture promote tumor proliferation and metastasis and are linked to a worse clinical outcome (Schedin and Keely, 2011). In addition, ECM rigidity has been shown to promote invadopodia formation (Parekh et al., 2011) and high-density fibrillar collagen (HDFC) in particular increased invadopodia formation in the MDA-MB-231 breast cancer cell line (Artym et al., 2015).

bioRxiv preprint doi: https://doi.org/10.1101/2020.02.26.966762; this version posted February 27, 2020. The copyright holder for this preprint (which was not certified by peer review) is the author/funder, who has granted bioRxiv a license to display the preprint in perpetuity. It is made available under aCC-BY-NC-ND 4.0 International license.

We have previously published that Tks5 knockdown is not required for growth of either breast cancer or melanoma cells on tissue culture plastic, but has an inhibitory effect when cells are placed in a cross-linked matrix of type I collagen (collagen-I) (Blouw et al., 2015; Iizuka et al., 2016). An example of this finding is shown in **Figure 2A**. Over the course of this five-day assay, control cells increased in number approximately 10-fold, but knockdown of Tks5 with two different shRNAs had a marked inhibitory effect. Interestingly, the basement membrane surrogate Matrigel stimulated growth only three-fold over the same time period, although Tks5 knockdown was still inhibitory. We next wanted to explore whether the ability of collagen-I to form cross-links was important for the observed growth stimulation. To do this we compared native collagen to a pepsinized version which lacked the telopeptides where cross-linking occurred (**Figure 2B**). We found that, compared to controls, atelo-collagen only poorly stimulated growth, independent of Tks5 expression (**Figure 2C**). Atelocollagen was also unable to promote invadopodia formation in MDA-MB-231 cells and two other invasive breast cancer cell lines, Hs578t and HCC1806, when compared to native collagen-I (**Figure 2C**). These data are consistent with a report that fibrillar collagen-I induced an invasive phenotype in breast cancer cells whereas high-density non-fibrillar collagen-I (generated by sonication to shear fibrils) suppressed invasive behavior (Maller et al., 2013).

Epithelial cells interact with collagen via integrins (predominantly α1β1 and α2β1) and the receptor tyrosine kinases DDR1 and DDR2 (Leitinger and Hohenester, 2007), with the DDRs attracting recent attention as possible therapeutic targets (Brakebusch and Fassler, 2005; Rammal et al., 2016; Valiathan et al., 2012). DDR1 is reported to have a kinase-independent function in linearizing invadopodia (Juin et al., 2014). There are no reports on DDR2, although interestingly DDR2 is involved in hypoxia-stimulated invasion of cancer cells (Ren et al., 2014), through stabilization of Snail and subsequent EMT (Zhang et al., 2013). Hypoxia increases invadopodia formation (Diaz et al., 2013), as does Twist-stimulation (Eckert et al., 2011). This suggests a

bioRxiv preprint doi: https://doi.org/10.1101/2020.02.26.966762; this version posted February 27, 2020. The copyright holder for this preprint (which was not certified by peer review) is the author/funder, who has granted bioRxiv a license to display the preprint in perpetuity. It is made available under aCC-BY-NC-ND 4.0 International license.

335 possible reciprocal relationship between invadopodia and collagen-DDR signaling. We used two
336 approaches to investigate this. First, we knocked down DDR1 and DDR2, and tested the effect
337 on growth on and in collagen-I. In both cases we observed a reduction in collagen-I stimulated
338 growth, to the same extent as Tks5 knockdown (**Figure 2D**). Secondly, we evaluated the effect
339 of the DDR inhibitor DDR1-IN-1, which inhibits both DDR1 and DDR2 at the concentrations used
340 (Kim et al., 2013). We observed a reduction in the invasion and growth of breast cancer cells in
341 3D (using a spheroid assay), but not 2D growth (**Figure 2E**, not shown). Together, these data
342 highlight the importance of DDR signaling in invadopodia formation. It is likely that many of these
343 effects occur through DDR2, which is uniquely activated by fibrillar collagen-I (Itoh, 2018; Rammal
344 et al., 2016), whereas DDR1 can be activated by both collagen-I and collagen-IV lacking fibrillar
345 structure. This will be explored in more detail in future work.
346
347 ***The effect of ECM on invadopodia formation***.
348 Research in recent years has highlighted the importance of the tumor microenvironment on
349 invadopodia formation and function, but efforts to systematically evaluate how the
350 microenvironment regulates invadopodia have been hampered by its complexity. Aside from a
351 myriad of insoluble ECM components, the typical tumor microenvironment also consists of soluble
352 growth factors, cytokines and chemokines, secreted by multiple different cell types. With these
353 issues in mind, the Korkola laboratory has developed the microenvironmental microarray (MEMA)
354 technology to enable study of the microenvironment (Watson et al., 2018). MEMA consist of
355 arrayed combinations of ECM molecules printed into each well of a multi-well plate, where each
356 printed ECM spot forms a growth pad upon which cells can be cultured. Each individual well is
357 treated with a separate soluble growth factor or ligand. By performing these assays in a multi-well
358 format, the effects of unique combinations of ECM plus ligand can be assessed for their effects
359 on cellular phenotypes (Watson et al., 2018). We ran a small-scale MEMA experiment using MDA-
360 MB-231 cells in which expression of endogenous Tks5 was suppressed by RNA interference, and

bioRxiv preprint doi: https://doi.org/10.1101/2020.02.26.966762; this version posted February 27, 2020. The copyright holder for this preprint (which was not certified by peer review) is the author/funder, who has granted bioRxiv a license to display the preprint in perpetuity. It is made available under aCC-BY-NC-ND 4.0 International license.

361 replaced by similar levels of Tks5αGFP. We used 45 different ECM proteins, with either no ligand,
362 EGF, FGF or HGF, for a total of 192 different conditions in this screen. After 24 hours of growth,
363 cells were fixed and stained with phalloidin for F-actin visualization and Tks5α co-localization on
364 a confocal microscope (**Figure 3**). As expected, we observed collagen-I stimulation of
365 invadopodia formation. We also observed stimulation by laminin, consistent with known biology
366 and the observation that invadopodia form at contact sites with basement membrane
367 (Schoumacher et al., 2010). We also saw more invadopodia on fibronectin, an abundant ECM
368 protein with appreciated roles in cancer (Rick et al., 2019). But the most prominent ECM inducer
369 of invadopodia was tropoelastin, the soluble precursor of the cross-linked ECM protein elastin
370 (Vindin et al., 2019). As the name suggests, elastin provides elasticity and resilience to many
371 organs, including the breast and the lung (a frequent site of breast cancer metastasis). Pericellular
372 proteolysis of elastin can impact several aspects of cancer progression (Scandolera et al., 2016),
373 although a discrete role in invadopodia biology has not previously been reported. None of the
374 added growth factors were found to impact invadopodia formation in this MEMA assay format (not
375 shown). This small-scale study demonstrates the feasibility of MEMA to identify novel modulators
376 of invadopodia. In the future, it will be important to also test the roles of their corresponding
377 receptors and downstream signaling events on invadopodia biology.

378

379 ***Spatial distribution of Tks5α and other invadopodia components***.
380 Previous studies have started to reveal fundamental properties of invadopodia such as molecular
381 components, order of assembly, and overall architecture. Currently, it is thought that invadopodia
382 formation begins with a 'core' of branching cortical actin (with actin, cortactin, N-WASP, cofilin
383 and so on), likely through Src-mediated tyrosine phosphorylation of cortactin, followed by
384 recruitment of SHP2 and Tks5α (Oikawa et al., 2008; Sharma et al., 2013). SHP2 generates
385 PI(3,4)P2, which binds to the PX domain of Tks5α to turn the latter into a multi-functional scaffold

bioRxiv preprint doi: https://doi.org/10.1101/2020.02.26.966762; this version posted February 27, 2020. The copyright holder for this preprint (which was not certified by peer review) is the author/funder, who has granted bioRxiv a license to display the preprint in perpetuity. It is made available under aCC-BY-NC-ND 4.0 International license.

386 to: bind to and stabilize filamentous actin; allow protrusion extension and maturation; engage and
387 activate proteases such as the ADAMs and potentially MMPs for proteolytic activities; and recruit
388 other adaptor proteins such as Nck2 and dynamin-2, which help organize signaling molecules
389 such as the integrins, EGFR, and MET. While recruitment of these proteins and lipids could
390 explain the various biological functions of invadopodia, the prior studies have mostly used 2D
391 culture systems (e.g., on coverslips with or without a thin layer of gelatin). The structure and
392 dynamics of invadopodia in more physiological 3D growth conditions remain poorly defined. We
393 have conducted a series of experiments to define invadopodia in native collagen-I. Unexpectedly,
394 both in tumor cell spheroids in 3D and cells on HDFC, Tks5α localization was restricted at the
395 base of invadopodia but not in the protrusion body itself (**Figure 4A, B, E and Supplementary**
396 **movie1**). We have also used super-resolution microscopy (SRM) to image Tks5 and the results
397 revealed even more details of Tks5α distribution at the base of invadopodia, resembling that of
398 the actin cortex (**Figure 4D and E**). Since Tks5 likely acts as a scaffold for multiple proteins, this
399 localization pattern might also confine relevant biological processes to the base of invadopodia.

400

401 We next evaluated the spatial distribution of the invadopodia components and actin regulators
402 cortactin, N-WASP and fascin HDFC. To do this, cortactin, N-WASP or fascin-GFP fusion proteins
403 were overexpressed in MDA-MB-231 cells together with Tks5α-mCherry, and the localization of
404 these proteins in invadopodia formed on HDFC evaluated (**Figure 5A, B**). First, we confirmed
405 that Tks5αGFP and Tks5α-mCherry were colocalized at the base of invadopodia. N-WASP
406 accumulated in similar areas to Tks5α, consistent with reports of their association between N-
407 WASP and Tks5 (Oikawa et al., 2008). However, cortactin, which has also been reported to
408 associate with Tks5α (Crimaldi et al., 2009), extends much further into the invadopodia body than
409 Tks5α. Finally, while there was no localization or accumulation of fascin in invadopodia at day 2
410 on HDFC, some fascin was detected along the protrusions beginning at day 4. These distributions

bioRxiv preprint doi: https://doi.org/10.1101/2020.02.26.966762; this version posted February 27, 2020. The copyright holder for this preprint (which was not certified by peer review) is the author/funder, who has granted bioRxiv a license to display the preprint in perpetuity. It is made available under aCC-BY-NC-ND 4.0 International license.

411 are schematized in **Figure 5C**. It will be important to extend these observations to other
412 invadopodia proteins in the future, and to look at the ultrastructure of the F-actin contained in
413 invadopodia over time. However, these observations may suggest that fascin-directed actin
414 cables only form once the protrusions have fully elongated.

415

416 ***Localization and function of pericellular proteases***

417 Invadopodia are known to be sites of pericellular proteolysis, with matrix, cysteine and serine
418 protease activity associated with them, although whether protease activity is required for
419 invadopodia formation, or just for function, may be cell type and context dependent (Linder, 2007;
420 Murphy and Courtneidge, 2011). Nor have 3D studies of proteolytic activity associated with
421 invadopodia been performed. We have begun to investigate this by determining the localization
422 of both the MMPs and the cysteine cathepsins, initially focusing on their proteolytically active
423 forms, using activity based probes (ABPs) for cathepsins (Xiao et al., 2013) and MMPs
424 (Saghatelian et al., 2004). In both cases, active enzyme was localized to the base of invadopodia,
425 in approximately the same location as Tks5α in magnified orthogonal views (**Figure 6A and C)**.
426 3D sideview of invadopodia more clearly showed the spatial localization of those proteins
427 **(Figure6B, 6D, Supplementary movie2 and movie3)**. This was surprising, since it might have
428 been expected that ECM degradation occurs at the advancing tip of the invadopodium. It has
429 been shown that pericellular proteases can be delivered as exosome cargo to invadopodia
430 (Hoshino et al., 2013). In the future, it will be interesting to visualize exosomes and other
431 microvesicles in these 3D systems.

432

433 We next looked at the requirement for metalloprotease and cysteine cathepsin activity for
434 invadopodia formation, using small molecule inhibitors. We found that 3D growth was affected by
435 the MMP inhibitor GM6001 and the impermeable cathepsin inhibitor CA074 (**Figure 7A**). These

bioRxiv preprint doi: https://doi.org/10.1101/2020.02.26.966762; this version posted February 27, 2020. The copyright holder for this preprint (which was not certified by peer review) is the author/funder, who has granted bioRxiv a license to display the preprint in perpetuity. It is made available under aCC-BY-NC-ND 4.0 International license.

data suggest non-redundant, or concerted, functions for these two classes of protease. We used our high-resolution microscopy techniques to investigate further, comparing to a Src family kinase (SFK) inhibitor SU11333 (Laird et al., 2003), a derivative of SU6656 (Blake et al., 2000), since many invadopodia proteins are Src substrates (Murphy and Courtneidge, 2011). SFK inhibition markedly reduced the Tks5α content at the base of nascent invadopodia, whereas MMP and cathepsin inhibition caused an increase in Tks5α content (**Figure 7B and C).** We confirmed these observations by plotting signal intensities with z-stack depth (**Figure 7C, right**). SFK inhibition reduced both actin and Tks5α signals at invadopodia (Y-axis), but MMPs/cathepsin inhibition increased Tks5α accumulation at invadopodia compare to the DMSO control group. These graphs also show the decrease of protrusion depth (X-axis, actin intensity) in all inhibitor groups. To test the formation of functional invadopodia on HDFC, the length of invadopodia was measured. We found that all inhibitors markedly reduced the length of protrusions (**Figure 7D**). Thus, we speculate that SFK signaling may be required for initiation and perhaps maintenance of protrusions, whereas MMPs and cathepsins may promote the maturation/elongation of the structures.

CONCLUSIONS

In conclusion, we describe here two new antibodies: one (G6) recognizes all isoforms of Tks5; and one (F4) is specific for Tks5α. Both have antigen recognition utility in multiple formats including immunoblotting, immunoprecipitation and immunostaining (both immunohistochemistry and immunocytochemistry), making them highly valuable to the invadosome community. Combining these antibodies with several cutting-edge technologies such as super-resolution microscopy, MEMA and activity-based probes, we have begun to investigate the structure and function of invadopodia forming in response to the ECM. The results revealed new and complex sub-invadopodia architecture unseen in our previous analyses in 2D, and ECM components (tropoelastin) as novel invadopodia inducer. Among others, it is possible to evaluate whether

bioRxiv preprint doi: https://doi.org/10.1101/2020.02.26.966762; this version posted February 27, 2020. The copyright holder for this preprint (which was not certified by peer review) is the author/funder, who has granted bioRxiv a license to display the preprint in perpetuity. It is made available under aCC-BY-NC-ND 4.0 International license.

462 invadopodia architecture is influenced by the ECM components present by studying invadopodia
463 structure in 3D or semi-3D model systems. The 3D and HDFC formats also revealed that ECM
464 stimulates cancer cell growth in an invadopodia-dependent manner, which goes a long way to
465 explaining why Tks5α (and other invadopodia proteins) are required for growth of many invasive
466 cancer cells in 3D, but not when the same cells are cultured on tissue culture plastic.
467 Future studies will expand on the findings described herein, with the goals being to evaluate more
468 invadopodia components, to map their localizations, interactions and functionality. These studies
469 will be important to determine whether invadopodia initiators such as the DDR receptors co-
470 localize to invadopodia, as well as the spatial localization of their downstream signaling
471 components.
472

473 **ACKNOWLEDGMENTS**

474 We acknowledge the expert assistance of Dr. Stefanie Kaech Petrie and Crystal Chaw (cell
475 imaging) in the Advanced Multiscale Microscopy Shared Resource, Dr. Philip R Streeter and
476 YongPing Zhong (G6 antibody production) Oregon Stem Cell Center, Monoclonal Antibody Core,
477 and Dr. David Kilburn (MEMA preparation) in the Department of Biomedical Engineering, Knight
478 Cancer Institute at the OHSU. We also thank Dr. Ting Zheng for assistance with conjugating
479 antibodies used in DNA-PAINT experiments.
480 This work was supported in part by the National Institutes of Health grant R01 CA217625 and
481 support from the Knight Cancer Institute (SAC), Brenden Colson Center for Pancreatic Care at
482 OHSU (SLG).
483
484

485 **REFERENCES**

bioRxiv preprint doi: https://doi.org/10.1101/2020.02.26.966762; this version posted February 27, 2020. The copyright holder for this preprint (which was not certified by peer review) is the author/funder, who has granted bioRxiv a license to display the preprint in perpetuity. It is made available under aCC-BY-NC-ND 4.0 International license.

Abram, C.L., Seals, D.F., Pass, I., Salinsky, D., Maurer, L., Roth, T.M., Courtneidge, S.A., 2003. The adaptor protein fish associates with members of the ADAMs family and localizes to podosomes of Src-transformed cells. J Biol Chem 278, 16844-16851.

Artym, V.V., 2016. Preparation of High-Density Fibrillar Collagen Matrices That Mimic Desmoplastic Tumor Stroma. Current protocols in cell biology 70, 10.19.11-10.19.11.

Artym, V.V., Kindzelskii, A.L., Chen, W.T., Petty, H.R., 2002. Molecular proximity of seprase and the urokinase-type plasminogen activator receptor on malignant melanoma cell membranes: dependence on beta1 integrins and the cytoskeleton. Carcinogenesis 23, 1593-1601.

Artym, V.V., Swatkoski, S., Matsumoto, K., Campbell, C.B., Petrie, R.J., Dimitriadis, E.K., Li, X., Mueller, S.C., Bugge, T.H., Gucek, M., Yamada, K.M., 2015. Dense fibrillar collagen is a potent inducer of invadopodia via a specific signaling network. J Cell Biol 208, 331-350.

Blake, R.A., Broome, M.A., Liu, X., Wu, J., Gishizky, M., Sun, L., Courtneidge, S.A., 2000. SU6656, a selective src family kinase inhibitor, used to probe growth factor signaling. Mol Cell Biol 20, 9018-9027.

Blouw, B., Patel, M., Iizuka, S., Abdullah, C., You, W.K., Huang, X., Li, J.L., Diaz, B., Stallcup, W.B., Courtneidge, S.A., 2015. The invadopodia scaffold protein Tks5 is required for the growth of human breast cancer cells in vitro and in vivo. PLoS One 10, e0121003.

Brakebusch, C., Fassler, R., 2005. beta 1 integrin function in vivo: adhesion, migration and more. Cancer Metastasis Rev 24, 403-411.

Buschman, M.D., Bromann, P.A., Cejudo-Martin, P., Wen, F., Pass, I., Courtneidge, S.A., 2009. The novel adaptor protein Tks4 (SH3PXD2B) is required for functional podosome formation. Mol Biol Cell 20, 1302-1311.

Cejudo-Martin, P., Yuen, A., Vlahovich, N., Lock, P., Courtneidge, S.A., Diaz, B., 2014. Genetic disruption of the sh3pxd2a gene reveals an essential role in mouse development and the existence of a novel isoform of tks5. PLoS One 9, e107674.

bioRxiv preprint doi: https://doi.org/10.1101/2020.02.26.966762; this version posted February 27, 2020. The copyright holder for this preprint (which was not certified by peer review) is the author/funder, who has granted bioRxiv a license to display the preprint in perpetuity. It is made available under aCC-BY-NC-ND 4.0 International license.

511 Chang, C., Werb, Z., 2001. The many faces of metalloproteases: cell growth, invasion,
512 angiogenesis and metastasis. Trends in cell biology 11, S37-43.
513 Chen, W.T., 1989. Proteolytic activity of specialized surface protrusions formed at rosette contact
514 sites of transformed cells. The Journal of experimental zoology 251, 167-185.
515 Creech, M.K., Wang, J., Nan, X., Gibbs, S.L., 2017. Superresolution Imaging of Clinical Formalin
516 Fixed Paraffin Embedded Breast Cancer with Single Molecule Localization Microscopy. Sci Rep
517 7, 40766.
518 Crimaldi, L., Courtneidge, S.A., Gimona, M., 2009. Tks5 recruits AFAP-110, p190RhoGAP, and
519 cortactin for podosome formation. Exp Cell Res 315, 2581-2592.
520 Diaz, B., Shani, G., Pass, I., Anderson, D., Quintavalle, M., Courtneidge, S.A., 2009. Tks5-
521 dependent, nox-mediated generation of reactive oxygen species is necessary for invadopodia
522 formation. Sci Signal 2, ra53.
523 Diaz, B., Yuen, A., Iizuka, S., Higashiyama, S., Courtneidge, S.A., 2013. Notch increases the
524 shedding of HB-EGF by ADAM12 to potentiate invadopodia formation in hypoxia. J Cell Biol 201,
525 279-292.
526 Eckert, M.A., Lwin, T.M., Chang, A.T., Kim, J., Danis, E., Ohno-Machado, L., Yang, J., 2011.
527 Twist1-induced invadopodia formation promotes tumor metastasis. Cancer Cell 19, 372-386.
528 Gligorijevic, B., Bergman, A., Condeelis, J., 2014. Multiparametric classification links tumor
529 microenvironments with tumor cell phenotype. PLoS biology 12, e1001995.
530 Hanahan, D., Weinberg, R.A., 2011. Hallmarks of cancer: the next generation. Cell 144, 646-674.
531 Hannant, J., Hedley, J.H., Pate, J., Walli, A., Farha Al-Said, S.A., Galindo, M.A., Connolly, B.A.,
532 Horrocks, B.R., Houlton, A., Pike, A.R., 2010. Modification of DNA-templated conductive polymer
533 nanowires via click chemistry. Chem Commun (Camb) 46, 5870-5872.
534 Henriet, P., Zhong, Z.D., Brooks, P.C., Weinberg, K.I., DeClerck, Y.A., 2000. Contact with fibrillar
535 collagen inhibits melanoma cell proliferation by up-regulating p27KIP1. Proc Natl Acad Sci U S A
536 97, 10026-10031.

bioRxiv preprint doi: https://doi.org/10.1101/2020.02.26.966762; this version posted February 27, 2020. The copyright holder for this preprint (which was not certified by peer review) is the author/funder, who has granted bioRxiv a license to display the preprint in perpetuity. It is made available under aCC-BY-NC-ND 4.0 International license.

537 Hoshino, D., Kirkbride, K.C., Costello, K., Clark, E.S., Sinha, S., Grega-Larson, N., Tyska, M.J.,
538 Weaver, A.M., 2013. Exosome secretion is enhanced by invadopodia and drives invasive
539 behavior. Cell reports 5, 1159-1168.
540 Huang, B., Wang, W., Bates, M., Zhuang, X., 2008. Three-dimensional super-resolution imaging
541 by stochastic optical reconstruction microscopy. Science 319, 810-813.
542 Iizuka, S., Abdullah, C., Buschman, M.D., Diaz, B., Courtneidge, S.A., 2016. The role of Tks
543 adaptor proteins in invadopodia formation, growth and metastasis of melanoma. Oncotarget 7,
544 78473-78486.
545 Itoh, Y., 2018. Discoidin domain receptors: Microenvironment sensors that promote cellular
546 migration and invasion. Cell adhesion & migration 12, 378-385.
547 Jacob, A., Linklater, E., Bayless, B.A., Lyons, T., Prekeris, R., 2016. The role and regulation of
548 Rab40b-Tks5 complex during invadopodia formation and cancer cell invasion. J Cell Sci 129,
549 4341-4353.
550 Juin, A., Di Martino, J., Leitinger, B., Henriet, E., Gary, A.S., Paysan, L., Bomo, J., Baffet, G.,
551 Gauthier-Rouviere, C., Rosenbaum, J., Moreau, V., Saltel, F., 2014. Discoidin domain receptor 1
552 controls linear invadosome formation via a Cdc42-Tuba pathway. J Cell Biol 207, 517-533.
553 Keely, P.J., 2011. Mechanisms by which the extracellular matrix and integrin signaling act to
554 regulate the switch between tumor suppression and tumor promotion. Journal of mammary gland
555 biology and neoplasia 16, 205-219.
556 Kelm, J.M., Timmins, N.E., Brown, C.J., Fussenegger, M., Nielsen, L.K., 2003. Method for
557 generation of homogeneous multicellular tumor spheroids applicable to a wide variety of cell
558 types. Biotechnol Bioeng 83, 173-180.
559 Kim, H.G., Tan, L., Weisberg, E.L., Liu, F., Canning, P., Choi, H.G., Ezell, S.A., Wu, H., Zhao, Z.,
560 Wang, J., Mandinova, A., Griffin, J.D., Bullock, A.N., Liu, Q., Lee, S.W., Gray, N.S., 2013.
561 Discovery of a potent and selective DDR1 receptor tyrosine kinase inhibitor. ACS Chem Biol 8,
562 2145-2150.

bioRxiv preprint doi: https://doi.org/10.1101/2020.02.26.966762; this version posted February 27, 2020. The copyright holder for this preprint (which was not certified by peer review) is the author/funder, who has granted bioRxiv a license to display the preprint in perpetuity. It is made available under aCC-BY-NC-ND 4.0 International license.

563 Kohler, G., Milstein, C., 1975. Continuous cultures of fused cells secreting antibody of predefined
564 specificity. Nature 256, 495-497.
565 Laird, A.D., Li, G., Moss, K.G., Blake, R.A., Broome, M.A., Cherrington, J.M., Mendel, D.B., 2003.
566 Src family kinase activity is required for signal tranducer and activator of transcription 3 and focal
567 adhesion kinase phosphorylation and vascular endothelial growth factor signaling in vivo and for
568 anchorage-dependent and -independent growth of human tumor cells. Mol Cancer Ther 2, 461-
569 469.
570 Leitinger, B., Hohenester, E., 2007. Mammalian collagen receptors. Matrix biology : journal of the
571 International Society for Matrix Biology 26, 146-155.
572 Leong, H.S., Robertson, A.E., Stoletov, K., Leith, S.J., Chin, C.A., Chien, A.E., Hague, M.N.,
573 Ablack, A., Carmine-Simmen, K., McPherson, V.A., Postenka, C.O., Turley, E.A., Courtneidge,
574 S.A., Chambers, A.F., Lewis, J.D., 2014. Invadopodia are required for cancer cell extravasation
575 and are a therapeutic target for metastasis. Cell reports 8, 1558-1570.
576 Li, C.M., Chen, G., Dayton, T.L., Kim-Kiselak, C., Hoersch, S., Whittaker, C.A., Bronson, R.T.,
577 Beer, D.G., Winslow, M.M., Jacks, T., 2013. Differential Tks5 isoform expression contributes to
578 metastatic invasion of lung adenocarcinoma. Genes & development 27, 1557-1567.
579 Linder, S., 2007. The matrix corroded: podosomes and invadopodia in extracellular matrix
580 degradation. Trends in cell biology 17, 107-117.
581 Linder, S., Wiesner, C., Himmel, M., 2011. Degrading devices: invadosomes in proteolytic cell
582 invasion. Annual review of cell and developmental biology 27, 185-211.
583 Lock, P., Abram, C.L., Gibson, T., Courtneidge, S.A., 1998. A new method for isolating tyrosine
584 kinase substrates used to identify fish, an SH3 and PX domain-containing protein, and Src
585 substrate. EMBO J 17, 4346-4357.
586 Lu, P., Weaver, V.M., Werb, Z., 2012. The extracellular matrix: a dynamic niche in cancer
587 progression. J Cell Biol 196, 395-406.

bioRxiv preprint doi: https://doi.org/10.1101/2020.02.26.966762; this version posted February 27, 2020. The copyright holder for this preprint (which was not certified by peer review) is the author/funder, who has granted bioRxiv a license to display the preprint in perpetuity. It is made available under aCC-BY-NC-ND 4.0 International license.

588 Lukinavicius, G., Umezawa, K., Olivier, N., Honigmann, A., Yang, G., Plass, T., Mueller, V.,
589 Reymond, L., Correa, I.R., Jr., Luo, Z.G., Schultz, C., Lemke, E.A., Heppenstall, P., Eggeling, C.,
590 Manley, S., Johnsson, K., 2013. A near-infrared fluorophore for live-cell super-resolution
591 microscopy of cellular proteins. Nat Chem 5, 132-139.
592 Luxenburg, C., Geblinger, D., Klein, E., Anderson, K., Hanein, D., Geiger, B., Addadi, L., 2007.
593 The architecture of the adhesive apparatus of cultured osteoclasts: from podosome formation to
594 sealing zone assembly. PLoS One 2, e179.
595 Maller, O., Hansen, K.C., Lyons, T.R., Acerbi, I., Weaver, V.M., Prekeris, R., Tan, A.C., Schedin,
596 P., 2013. Collagen architecture in pregnancy-induced protection from breast cancer. J Cell Sci
597 126, 4108-4110.
598 Monsky, W.L., Lin, C.Y., Aoyama, A., Kelly, T., Akiyama, S.K., Mueller, S.C., Chen, W.T., 1994.
599 A potential marker protease of invasiveness, seprase, is localized on invadopodia of human
600 malignant melanoma cells. Cancer Res 54, 5702-5710.
601 Murphy, D.A., Courtneidge, S.A., 2011. The 'ins' and 'outs' of podosomes and invadopodia:
602 characteristics, formation and function. Nat Rev Mol Cell Biol 12, 413-426.
603 Murphy, D.A., Diaz, B., Bromann, P.A., Tsai, J.H., Kawakami, Y., Maurer, J., Stewart, R.A.,
604 Izpisua-Belmonte, J.C., Courtneidge, S.A., 2011. A Src-Tks5 pathway is required for neural crest
605 cell migration during embryonic development. PLoS One 6, e22499.
606 Oikawa, T., Itoh, T., Takenawa, T., 2008. Sequential signals toward podosome formation in NIH-
607 src cells. J Cell Biol 182, 157-169.
608 Ovesny, M., Krizek, P., Borkovec, J., Svindrych, Z., Hagen, G.M., 2014. ThunderSTORM: a
609 comprehensive ImageJ plug-in for PALM and STORM data analysis and super-resolution
610 imaging. Bioinformatics 30, 2389-2390.
611 Parekh, A., Ruppender, N.S., Branch, K.M., Sewell-Loftin, M.K., Lin, J., Boyer, P.D., Candiello,
612 J.E., Merryman, W.D., Guelcher, S.A., Weaver, A.M., 2011. Sensing and modulation of
613 invadopodia across a wide range of rigidities. Biophysical journal 100, 573-582.

bioRxiv preprint doi: https://doi.org/10.1101/2020.02.26.966762; this version posted February 27, 2020. The copyright holder for this preprint (which was not certified by peer review) is the author/funder, who has granted bioRxiv a license to display the preprint in perpetuity. It is made available under aCC-BY-NC-ND 4.0 International license.

614 Pickup, M.W., Mouw, J.K., Weaver, V.M., 2014. The extracellular matrix modulates the hallmarks
615 of cancer. EMBO reports 15, 1243-1253.
616 Quintavalle, M., Elia, L., Condorelli, G., Courtneidge, S.A., 2010. MicroRNA control of podosome
617 formation in vascular smooth muscle cells in vivo and in vitro. J Cell Biol 189, 13-22.
618 Rammal, H., Saby, C., Magnien, K., Van-Gulick, L., Garnotel, R., Buache, E., El Btaouri, H.,
619 Jeannesson, P., Morjani, H., 2016. Discoidin Domain Receptors: Potential Actors and Targets in
620 Cancer. Front Pharmacol 7, 55.
621 Ren, T., Zhang, W., Liu, X., Zhao, H., Zhang, J., Zhang, J., Li, X., Zhang, Y., Bu, X., Shi, M., Yao,
622 L., Su, J., 2014. Discoidin domain receptor 2 (DDR2) promotes breast cancer cell metastasis and
623 the mechanism implicates epithelial-mesenchymal transition programme under hypoxia. The
624 Journal of pathology 234, 526-537.
625 Rick, J.W., Chandra, A., Dalle Ore, C., Nguyen, A.T., Yagnik, G., Aghi, M.K., 2019. Fibronectin in
626 malignancy: Cancer-specific alterations, protumoral effects, and therapeutic implications. Semin
627 Oncol 46, 284-290.
628 Rufer, A.C., Rumpf, J., von Holleben, M., Beer, S., Rittinger, K., Groemping, Y., 2009. Isoform-
629 selective interaction of the adaptor protein Tks5/FISH with Sos1 and dynamins. J Mol Biol 390,
630 939-950.
631 Saghatelian, A., Jessani, N., Joseph, A., Humphrey, M., Cravatt, B.F., 2004. Activity-based
632 probes for the proteomic profiling of metalloproteases. Proc Natl Acad Sci U S A 101, 10000-
633 10005.
634 Saini, P., Courtneidge, S.A., 2018. Tks adaptor proteins at a glance. J Cell Sci 131.
635 Scandolera, A., Odoul, L., Salesse, S., Guillot, A., Blaise, S., Kawecki, C., Maurice, P., El Btaouri,
636 H., Romier-Crouzet, B., Martiny, L., Debelle, L., Duca, L., 2016. The Elastin Receptor Complex:
637 A Unique Matricellular Receptor with High Anti-tumoral Potential. Front Pharmacol 7, 32.

bioRxiv preprint doi: https://doi.org/10.1101/2020.02.26.966762; this version posted February 27, 2020. The copyright holder for this preprint (which was not certified by peer review) is the author/funder, who has granted bioRxiv a license to display the preprint in perpetuity. It is made available under aCC-BY-NC-ND 4.0 International license.

638 Schedin, P., Keely, P.J., 2011. Mammary gland ECM remodeling, stiffness, and
639 mechanosignaling in normal development and tumor progression. Cold Spring Harb Perspect Biol
640 3, a003228.
641 Schnitzbauer, J., Strauss, M.T., Schlichthaerle, T., Schueder, F., Jungmann, R., 2017. Super-
642 resolution microscopy with DNA-PAINT. Nat Protoc 12, 1198-1228.
643 Schoumacher, M., Goldman, R.D., Louvard, D., Vignjevic, D.M., 2010. Actin, microtubules, and
644 vimentin intermediate filaments cooperate for elongation of invadopodia. J Cell Biol 189, 541-556.
645 Seals, D.F., Azucena, E.F., Jr., Pass, I., Tesfay, L., Gordon, R., Woodrow, M., Resau, J.H.,
646 Courtneidge, S.A., 2005. The adaptor protein Tks5/Fish is required for podosome formation and
647 function, and for the protease-driven invasion of cancer cells. Cancer Cell 7, 155-165.
648 Seals, D.F., Courtneidge, S.A., 2003. The ADAMs family of metalloproteases: multidomain
649 proteins with multiple functions. Genes & development 17, 7-30.
650 Sharma, V.P., Eddy, R., Entenberg, D., Kai, M., Gertler, F.B., Condeelis, J., 2013. Tks5 and
651 SHIP2 regulate invadopodium maturation, but not initiation, in breast carcinoma cells. Current
652 biology : CB 23, 2079-2089.
653 Smith, R., Devlin, K., Kilburn, D., Gross, S., Sudar, D., Bucher, E., Nederlof, M., Dane, M., Gray,
654 J.W., Heiser, L., Korkola, J.E., 2019. Using Microarrays to Interrogate Microenvironmental Impact
655 on Cellular Phenotypes in Cancer. J Vis Exp.
656 Stylli, S.S., Stacey, T.T., Verhagen, A.M., Xu, S.S., Pass, I., Courtneidge, S.A., Lock, P., 2009.
657 Nck adaptor proteins link Tks5 to invadopodia actin regulation and ECM degradation. J Cell Sci
658 122, 2727-2740.
659 Tarone, G., Cirillo, D., Giancotti, F.G., Comoglio, P.M., Marchisio, P.C., 1985. Rous sarcoma
660 virus-transformed fibroblasts adhere primarily at discrete protrusions of the ventral membrane
661 called podosomes. Exp Cell Res 159, 141-157.
662 Tu, C., Ortega-Cava, C.F., Chen, G., Fernandes, N.D., Cavallo-Medved, D., Sloane, B.F., Band,
663 V., Band, H., 2008. Lysosomal cathepsin B participates in the podosome-mediated extracellular

bioRxiv preprint doi: https://doi.org/10.1101/2020.02.26.966762; this version posted February 27, 2020. The copyright holder for this preprint (which was not certified by peer review) is the author/funder, who has granted bioRxiv a license to display the preprint in perpetuity. It is made available under aCC-BY-NC-ND 4.0 International license.

matrix degradation and invasion via secreted lysosomes in v-Src fibroblasts. Cancer Res 68, 9147-9156.

Valiathan, R.R., Marco, M., Leitinger, B., Kleer, C.G., Fridman, R., 2012. Discoidin domain receptor tyrosine kinases: new players in cancer progression. Cancer Metastasis Rev 31, 295-321.

van de Linde, S., Loschberger, A., Klein, T., Heidbreder, M., Wolter, S., Heilemann, M., Sauer, M., 2011. Direct stochastic optical reconstruction microscopy with standard fluorescent probes. Nat Protoc 6, 991-1009.

Vindin, H., Mithieux, S.M., Weiss, A.S., 2019. Elastin architecture. Matrix biology : journal of the International Society for Matrix Biology 84, 4-16.

Watson, S.S., Dane, M., Chin, K., Tatarova, Z., Liu, M., Liby, T., Thompson, W., Smith, R., Nederlof, M., Bucher, E., Kilburn, D., Whitman, M., Sudar, D., Mills, G.B., Heiser, L.M., Jonas, O., Gray, J.W., Korkola, J.E., 2018. Microenvironment-Mediated Mechanisms of Resistance to HER2 Inhibitors Differ between HER2+ Breast Cancer Subtypes. Cell Syst 6, 329-342 e326.

Weaver, A.M., 2008a. Cortactin in tumor invasiveness. Cancer Lett 265, 157-166.

Weaver, A.M., 2008b. Invadopodia. Current biology : CB 18, R362-364.

Xiao, J., Broz, P., Puri, A.W., Deu, E., Morell, M., Monack, D.M., Bogyo, M., 2013. A coupled protein and probe engineering approach for selective inhibition and activity-based probe labeling of the caspases. J Am Chem Soc 135, 9130-9138.

Zhang, K., Corsa, C.A., Ponik, S.M., Prior, J.L., Piwnica-Worms, D., Eliceiri, K.W., Keely, P.J., Longmore, G.D., 2013. The collagen receptor discoidin domain receptor 2 stabilizes SNAIL1 to facilitate breast cancer metastasis. Nat Cell Biol 15, 677-687.

bioRxiv preprint doi: https://doi.org/10.1101/2020.02.26.966762; this version posted February 27, 2020. The copyright holder for this preprint (which was not certified by peer review) is the author/funder, who has granted bioRxiv a license to display the preprint in perpetuity. It is made available under aCC-BY-NC-ND 4.0 International license.

FIGURE LEGENDS

Figure 1. Tks5 antibodies against PX domain (F4) and linker region (G6).

A Schematic view of Tks5 isoforms and antibody epitope regions. **B** Antibody specificity analyzed by immunoblotting on extracts from 293T cells transiently expressing full-length of Tks5α (Tks5), Tks5α with PX domain deletion (Δ PX) or full-length of Tks4 (Tks4). **C** Tks5 protein levels analyzed by immunoblotting on human breast cancer cell lines. Asterisks show predicted size of Tks5α (*) and Tks5β/short (**). Tubulin is shown as a loading control. **D and E** Validation of antibodies by immunofluorescence. (D) All Tks5 isoforms were stained by G6 in MDA-MB-231 cells with shRNA-scrambled (Ctrl), shRNA-Tks5 (D6) or shRNA-Tks5 (D7). Invadopodia were visualized by Tks5 (G6, green) and actin (phalloidin, red). (E) Tks5α was stained by F4 in Src-transformed NIH3T3 cells with Tks5αGFP overexpression. Magnified areas (1 and 2, orange square in top) were shown. Arrows show Tks5 accumulation at invadopodia. Arrowheads show Tks5α signals on microtubules in cytoplasmic region. **F** Invadopodia were stained for Tks5 (G6 or F4, red) and actin (phalloidin, green) in MDA-MB-231 cells. Magnified orthogonal views (orange square) were shown in left. Hoechst to denote nuclei of cells in the images. Scale bars, 5 μm (D, E left, F top) and 2 μm (E right, F bottom).

Figure 2. Crosstalk between invadopodia and the extracellular matrix.

A Growth of cells as indicated in the figure in 3D native type I collagen (3D native COLI) and in 3D matrigel (3D matrigel). Red line shows the cell number when they were embedded in matrix. **B** Schematic view of native collagen and atelocollagen. **C** Growth of cells as indicated in the figure on native type I collagen (native COLI) and atelocollagen (atelo COLI). Fold change in cell number in MDA-MB-231 cells with shRNA-scrambled (Ctrl), shRNA-Tks5 (D6), shRNA-Tks5 (D7) or shRNA-Tks5-D6 + rescued expression of Tks5αGFP (D6R) and representative images (actin by phalloidin) in MDA-MB-231, Hs578t or HCC1806 cells on each conditions (right). **D** Growth of

bioRxiv preprint doi: https://doi.org/10.1101/2020.02.26.966762; this version posted February 27, 2020. The copyright holder for this preprint (which was not certified by peer review) is the author/funder, who has granted bioRxiv a license to display the preprint in perpetuity. It is made available under aCC-BY-NC-ND 4.0 International license.

712 cells as indicated in the figure on high-dense type I collagen (HDFC) and in 3D native type I
713 collagen (3D native COLI). Fold change in cell number in MDA-MB-231 cells with shRNA-
714 scrambled (Ctrl), shRNA-Tks5 (D6), shRNA-Tks5-D6 with rescued expression of Tks5αGFP
715 (D6R) or shRNA-DDR1/2 (DDR1/2). **E** 3D growth/invasion in a hanging droplet spheroid assay
716 with DDR inhibitor, DDR-IN-1. Representative images of spheroids in type I collagen stained by
717 phalloidin (left) and spheroid size measured by actin intensity (right). Scale bars, 5 μm (C) and
718 500 μm (E). *P*>0.05 unless other specified; *, *P*<0.05; **, *P*<0.01; ***, *P*<0.001.
719
720 **Figure 3. Invadopodia formation assay on microenvironmental microarray (MEMA).**
721 **A** Overall view from one of the MEMA assays with MDA-MB-231 cells. Invadopodia were
722 visualized by actin (phalloidin) and Tks5αGFP. **B** Representative zoom-in images from each spot
723 as indicated in the figure (type I collagen: COLI, fibronectin: FN, laminin: LAM and tropoelastin).
724 Magnified areas (orange square at top) shown at bottom. Hoechst staining reveals nuclei of cells
725 in the images. Scale bars, 500 μm (A) and 10 μm (B).
726
727 **Figure 4. Fine structures of invadopodia in 3D type I collagen.**
728 **A** Invadopodia were visualized in a 3D type I collagen hanging droplet spheroids. Representative
729 images of MDA-MB-231 spheroids stained by phalloidin (red) and Tks5αGFP (green). Magnified
730 areas (orange square in left) were shown in middle. Hoechst staining reveals nuclei of cells in the
731 images. Magnified orthogonal view (orange square in middle) shown at right. **B** Invadopodia in
732 MDA-MB-231 cells with Tks5αGFP were visualized on high-dense fibrillar collagen (HDFC).
733 Representative images of invadopodia stained by phalloidin (red), Tks5αGFP (green) and HDFC
734 (gray). Magnified orthogonal view (orange square in left and middle) shown in the middle and
735 atright. 3D reconstruction images were processed by using Imaris software (3D signal or spots,
736 bottom). **C** Invadopodia on HDFC were visualized by phalloidin (red) and Tks5αGFP (green).

bioRxiv preprint doi: https://doi.org/10.1101/2020.02.26.966762; this version posted February 27, 2020. The copyright holder for this preprint (which was not certified by peer review) is the author/funder, who has granted bioRxiv a license to display the preprint in perpetuity. It is made available under aCC-BY-NC-ND 4.0 International license.

737 Hoechst to denote nuclei of cells in the images. Magnified orthogonal view (orange square in left)
738 were shown in middle. Digital zoom-in image from single z-stack plane in middle (orange square)
739 was shown in right. **D** 3D super-resolution microscopy (SRM) image of invadopodia on HDFC.
740 Sample was prepared at same time as in C. **E** Comparison of invadopodia on HDFC between
741 confocal microscopy and SRM. Representative images and structural information as indicated in
742 the figure. Scale bars, 100 μm (A left), 10 μm (A middle), 5 μm (B top left, C left), 2 μm (A right,
743 B top middle) and 1 μm (B top right, B bottom three, C right three).
744
745 **Figure 5. Localization of invadopodia components on HDFC.**
746 **A** Invadopodia in MDA-MB-231 cells with Tks5αGFP and Tks5α-mCherry were visualized on
747 HDFC. Representative images of invadopodia stained by phalloidin (gray), Tks5α-mCherry (red)
748 and Tks5αGFP (green). Magnified orthogonal view (orange square in top) shown at bottom.
749 Digital zoom-in side-view image from single invadopodia in bottom (orange square) shown at
750 right. Dot-line shows the area of cell membrane. **B** Invadopodia side-view images in Tks5α-
751 mCherry overexpressing MDA-MB-231 cells with cortactin-GFP, N-WASP-GFP or fascin-GFP on
752 HDFC. **C** Schematic view of invadopodia with localization of invadopodia-related proteins in 3D.
753 Scale bars, 5 μm (A top) and 3 μm (A bottom).
754
755 **Figure 6. Localization of protease activity at invadopodia on HDFC.**
756 **A** MMP activity at Invadopodia in MDA-MB-231 cells with Tks5αGFP were visualized on HDFC.
757 Representative images of invadopodia stained by phalloidin (red), Tks5αGFP (green) and MMP
758 activity (gray, MMP-ABP). Magnified orthogonal view (orange square in left and middle) were
759 shown in middle and right. 3D reconstruction images were processed by using Imaris software
760 (3D signal or spots) and shown in bottom. **B** Cathepsin activity at invadopodia in MDA-MB-231
761 cells with Tks5αGFP was visualized on HDFC. Representative images of invadopodia stained by

bioRxiv preprint doi: https://doi.org/10.1101/2020.02.26.966762; this version posted February 27, 2020. The copyright holder for this preprint (which was not certified by peer review) is the author/funder, who has granted bioRxiv a license to display the preprint in perpetuity. It is made available under aCC-BY-NC-ND 4.0 International license.

762 phalloidin (red), Tks5α (green, F4 antibody) and cathepsin activity (gray, CTS-ABP). Magnified
763 orthogonal view (orange square in left and middle) shown in middle and at right. 3D reconstruction
764 images were processed by using Imaris software (3D signal or spots) and shown at bottom. Scale
765 bars, 5 μm (A left, C left, D), 2 μm (A right, C right) and 1 μm (B).
766
767 **Figure 7. Role of protease activities in 3D invadopodia.**
768 **A** 3D growth/invasion in a hanging droplet spheroid assay in MDA-MB-231 cells with inhibitors,
769 GM6001 or CA074. Representative brightfield images of spheroids in type I collagen (top) with
770 spheroid size measured by actin intensity (bottom). **B** Invadopodia in MDA-MB-231 cells with
771 Tks5αGFP were visualized on high-dense fibrillar collagen (HDFC). The cells were treated with
772 DMSO, SU11333 (1μM), GM6001 (10μM) or CA074 (10μM). Representative images of
773 invadopodia stained by phalloidin (red), Tks5αGFP (green) and HDFC (gray). Magnified
774 orthogonal view (orange square) shown in left two panels. **C** Images from B were processed for
775 3D reconstruction (3D spots) using Imaris software. Length (z-depth) and intensity of actin or
776 Tks5αGFP (from three representative invadopodia) was analyzed in each condition (C, right
777 graphs). Red dotted-line shows depth of actin intensity 10 in each condition. Green dotted-line
778 shows maximum intensity of Tks5αGFP in DMSO. **D** Individual invadopodia length was measured
779 using Imaris software. Scale bars, 5 μm (B left, C) and 1 μm (B right). $P>0.05$ unless other
780 specified; *, $P<0.001$.

bioRxiv preprint doi: https://doi.org/10.1101/2020.02.26.966762; this version posted February 27, 2020. The copyright holder for this preprint (which was not certified by peer review) is the author/funder, who has granted bioRxiv a license to display the preprint in perpetuity. It is made available under aCC-BY-NC-ND 4.0 International license.

Figure 1

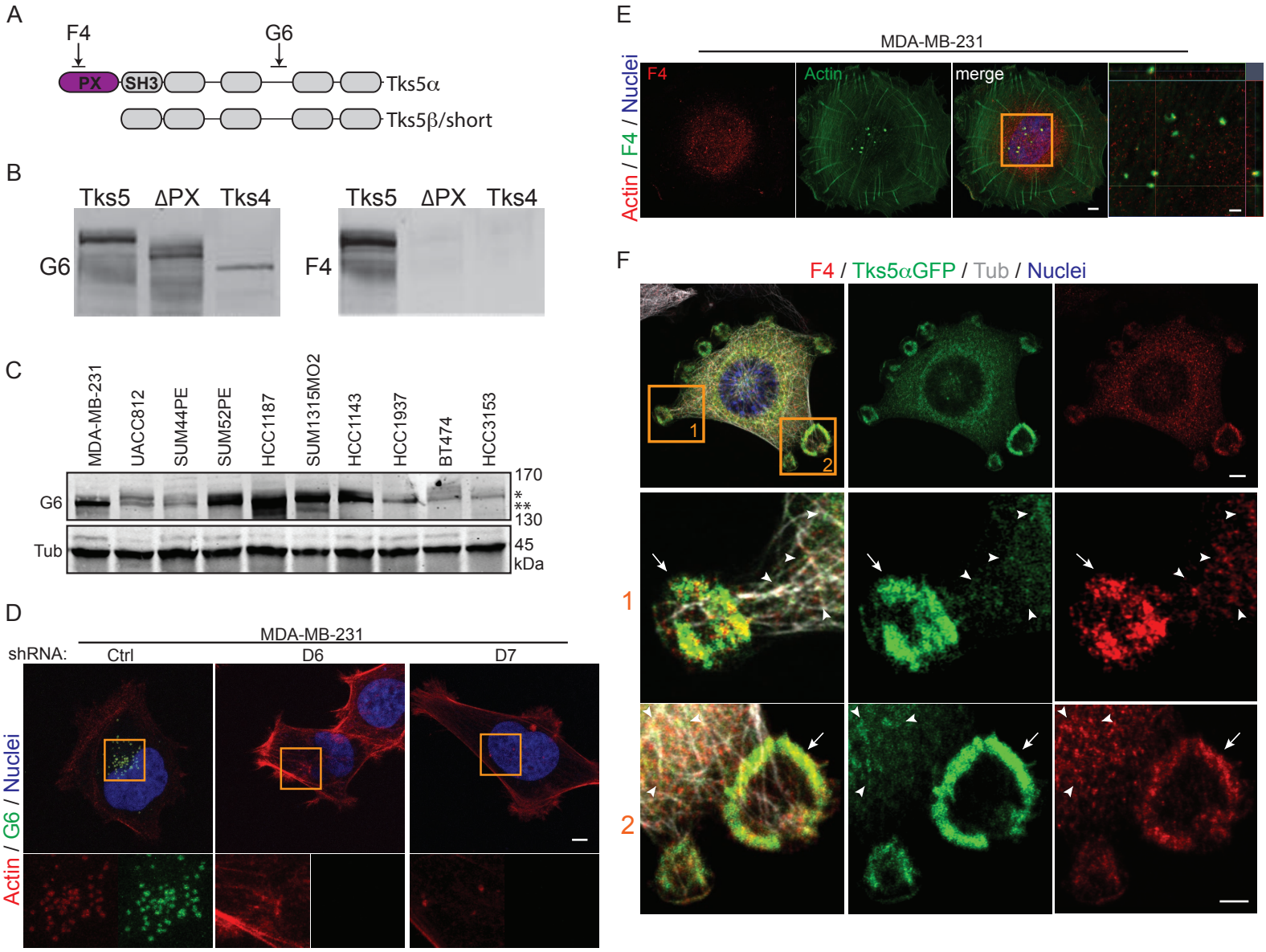

bioRxiv preprint doi: https://doi.org/10.1101/2020.02.26.966762; this version posted February 27, 2020. The copyright holder for this preprint (which was not certified by peer review) is the author/funder, who has granted bioRxiv a license to display the preprint in perpetuity. It is made available under aCC-BY-NC-ND 4.0 International license.

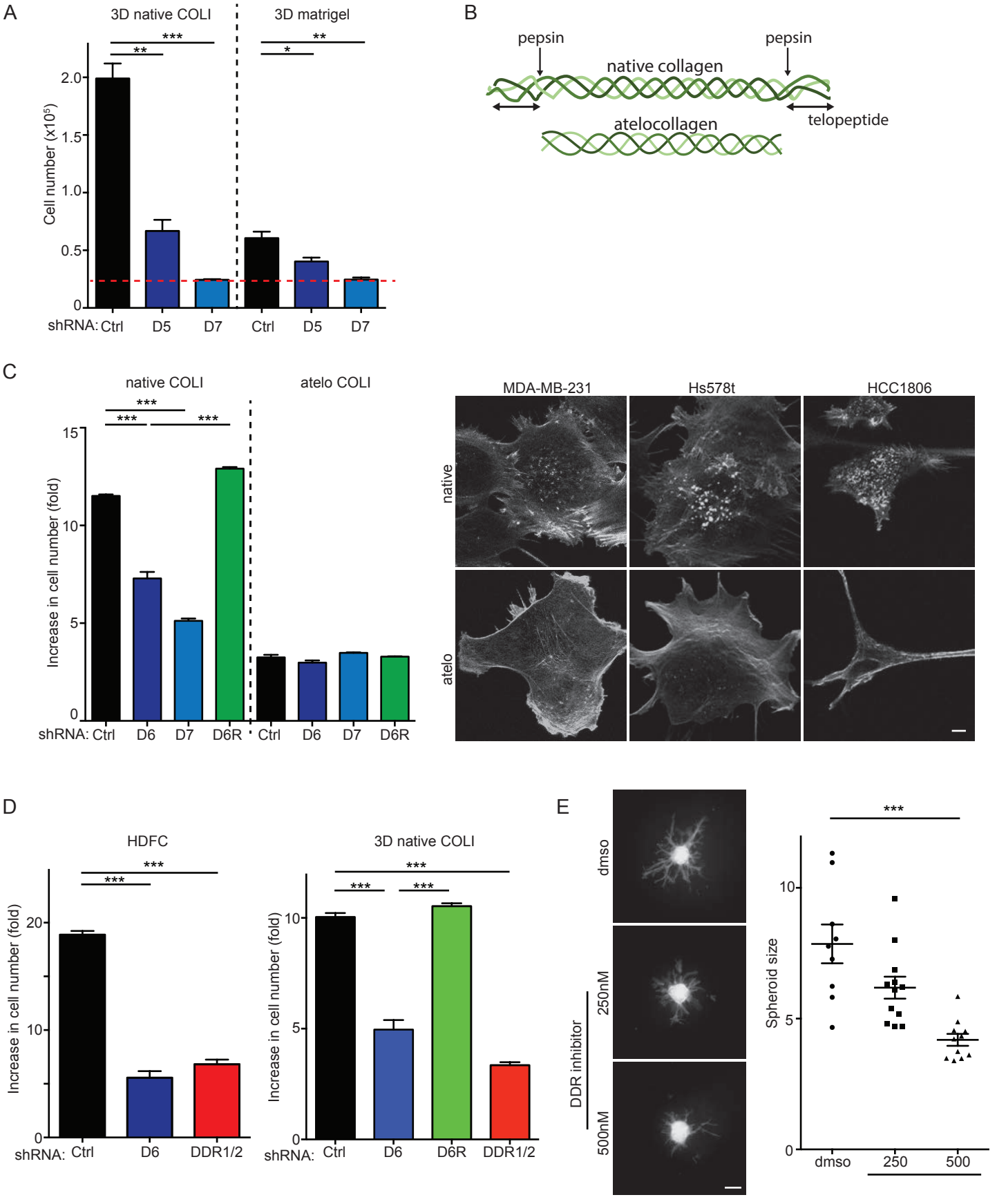

bioRxiv preprint doi: https://doi.org/10.1101/2020.02.26.966762; this version posted February 27, 2020. The copyright holder for this preprint (which was not certified by peer review) is the author/funder, who has granted bioRxiv a license to display the preprint in perpetuity. It is made available under aCC-BY-NC-ND 4.0 International license.

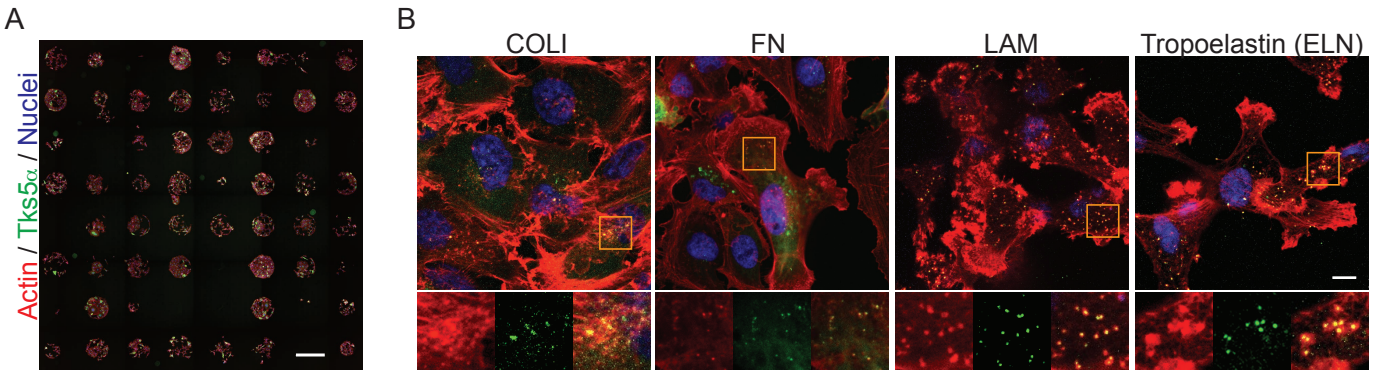

bioRxiv preprint doi: https://doi.org/10.1101/2020.02.26.966762; this version posted February 27, 2020. The copyright holder for this preprint (which was not certified by peer review) is the author/funder, who has granted bioRxiv a license to display the preprint in perpetuity. It is made available under aCC-BY-NC-ND 4.0 International license.

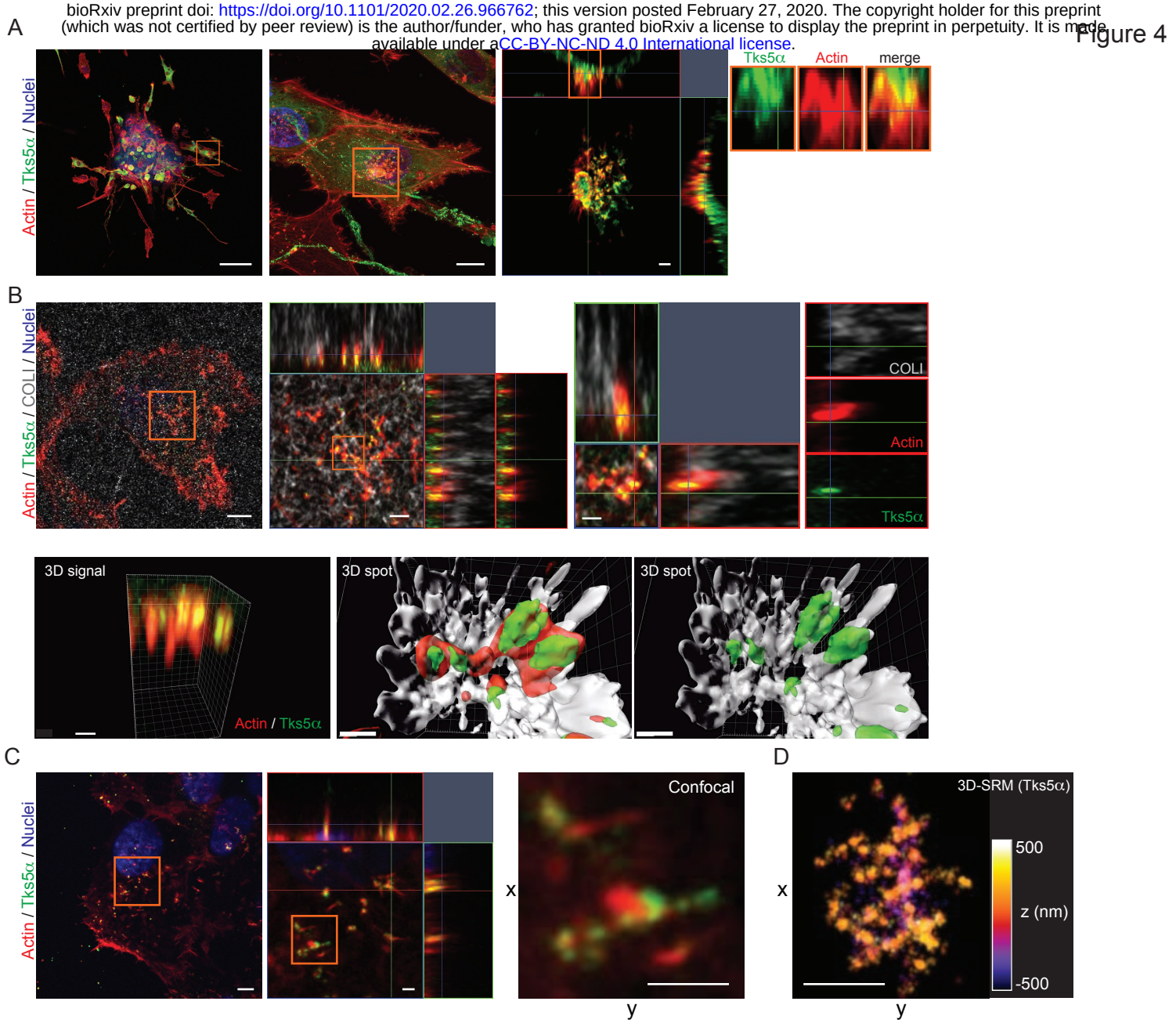

bioRxiv preprint doi: https://doi.org/10.1101/2020.02.26.966762; this version posted February 27, 2020. The copyright holder for this preprint (which was not certified by peer review) is the author/funder, who has granted bioRxiv a license to display the preprint in perpetuity. It is made available under aCC-BY-NC-ND 4.0 International license.

A

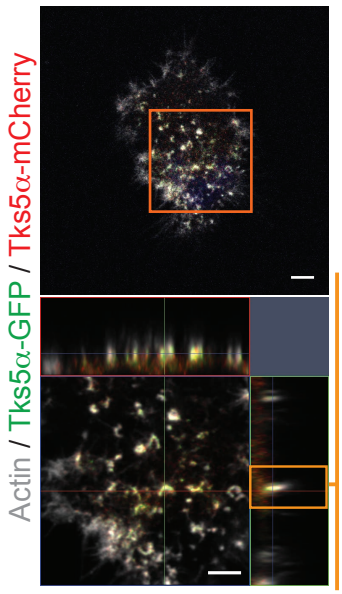

B

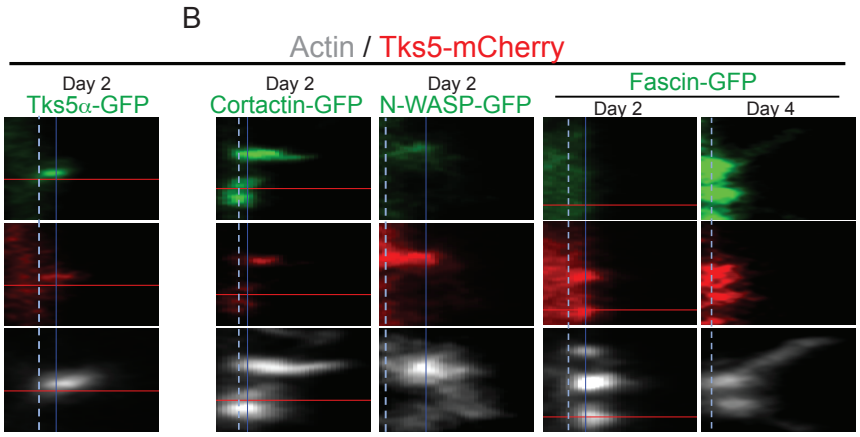

C

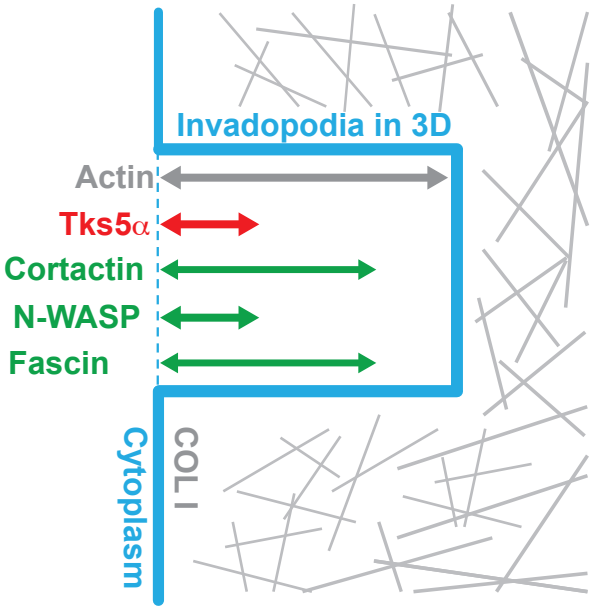

bioRxiv preprint doi: https://doi.org/10.1101/2020.02.26.966762; this version posted February 27, 2020. The copyright holder for this preprint (which was not certified by peer review) is the author/funder, who has granted bioRxiv a license to display the preprint in perpetuity. It is made available under aCC-BY-NC-ND 4.0 International license.

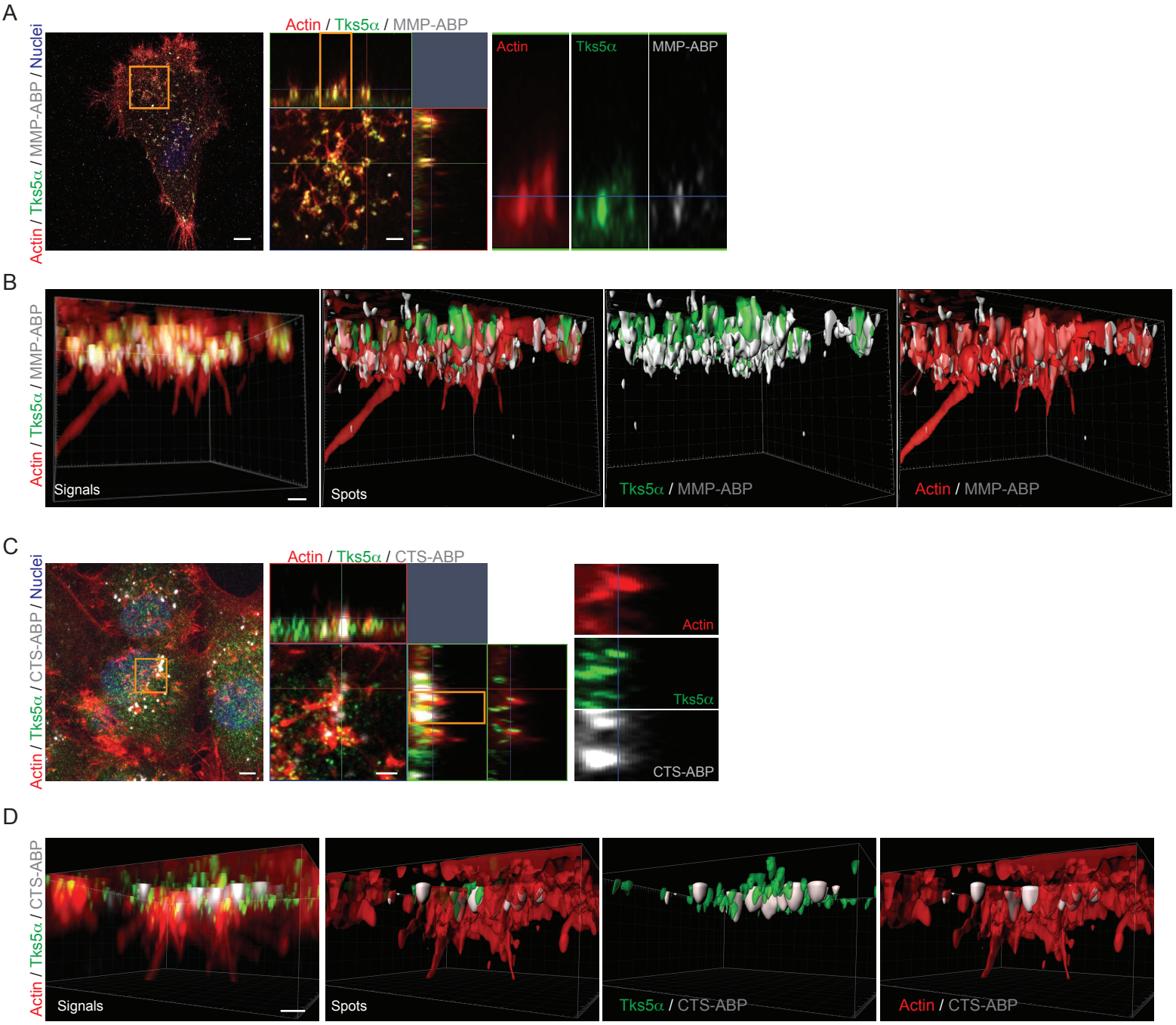

bioRxiv preprint doi: https://doi.org/10.1101/2020.02.26.966762; this version posted February 27, 2020. The copyright holder for this preprint (which was not certified by peer review) is the author/funder, who has granted bioRxiv a license to display the preprint in perpetuity. It is made available under aCC-BY-NC-ND 4.0 International license.